Available online at www.sciencedirect.com
ScienceDirect
Computer Physics Communications 178 (2008) 571–577
Computer Physics Communications
www.elsevier.com/locate/cpc

Calculation of atomic hydrogen and its photoelectron spectra in momentum space

T.F. Jiang

Institute of Physics, National Chiao-Tung University, Hsinchu 30010, Taiwan

Received 19 September 2007; received in revised form 12 November 2007; accepted 29 November 2007

Available online 23 December 2007

Abstract

An essential modification to the kernel in the numerical calculation of hydrogenic momentum wave functions, is presented in this paper. Using only 256 grid points, the calculated eigenvalues, eigenfunctions and the oscillator strengths are shown to be in excellent agreement with the exact analytic results. The reliable pseudocomplete set of momentum space eigenfunctions is then applied to the time-dependent calculation of intense laser pulse on the hydrogen atom. With the advantage of having no boundary reflection during the time evolution, like that inherent in the coordinate space method, the photoelectron spectra of above-threshold-ionization (ATI) are elucidated for four cases. Some of which are not feasible or very difficult to solve with the coordinate space method. Generalization of the method to single-active electron systems is straightforward. Due to the good accuracy with a reasonably small-sized basis set, applications to the currently interested intense case of laser pulse on atom or molecule are expected.

PACS: 31.15.-p; 03.65.Ca; 32.70.Cs

Keywords: Intense laser on atom; Momentum space; Photoelectron spectra; Above threshold ionization

1. Introduction

An atomic electron under intense laser fields may absorb many photons and photoionize. The above-threshold-ionization (ATI), first observed in 1979, is a phenomenon in which electron absorbs excess photons than is necessary to ionize [1]. Since then, the ATI has attracted much attention and interest [2,3]. Theoretically, the electron spectra can be calculated by solving the time-dependent Schrödinger equation, but this method is often limited by reflection from the boundary when the equation is solved in coordinate space. The trouble is less severe for shorter pulse where a large spatial region can be chosen such that the electron is still within the boundary when the laser pulse ends [4]. For stronger fields, the boundary reflection is still a problem even for few-cycle pulses. From the complementary principle of quantum mechanics, a wave function distributed in a large coordinate space corresponds to a wave function localized in momentum space. Using the momentum wave functions as a basis set to study atoms/molecules in laser fields, one would be able to avoid the trouble of boundary reflection. We have previously shown that the low-order ATI phenomenon is described rather well by the momentum space method [5].

In this paper, we find a more efficient and accurate momentum space method than our previous work. Although the formulation of Schrödinger equation in momentum space is well known [6], the number of analytic eigenfunctions is infinite and cannot be used directly in the simulation of time-dependent problems. There were efforts in developing the momentum space solution: Lande invented a regularization method for the Coulomb kernel singularity [7], Ivanov and Mitroy [8] designed the iteration codes for the expansion of the kernel, Norbury et al. [9] applied the specific basis function forms to the bound states, and Tang et al. [10] used the Bystrom method for the Coulomb kernel related integration and solved some of the bound states. For numerical calculations within a finite range, we find that the earlier formalism must be modified. Our key correction to the Coulomb kernel in practical compu-

E-mail address: tfjiang@faculty.nctu.edu.tw.

0010-4655/$ – see front matter
doi:10.1016/j.cpc.2007.11.019

tations makes the calculated energy levels and wave functions much more accurate. Another key improvement is the use of pseudospectral collocation points and a nonlinear mapping into momentum grids [11]. This mapping enables us to adjust the grids nonuniformly and optimize the favored region.

The goal of this paper is to present an efficient and accurate enough method of momentum space eigenstates calculation, and then use it as the basis set in the study of a hydrogen atom under intense laser fields. The computation of this time-dependent Schrödinger equation (TDSE) for pulse duration of hundreds optical cycles was thought impossible before [12], but with our method, it can be calculated easily with a modest desktop PC. This method can also be generalized straightforwardly to quantum systems modeled by a single-active-electron system under intense laser pulse. To illustrate the new development, we computed and compared the bound state levels and several radial momentum wave functions with the known analytical results. We tabulated the oscillator strengths for states $1s$, $2s$, $3s$, $4s$, $2p$ and $4f$ and compared them with the exact results listed in Bethe and Salpeter's [13]. The summation over discrete states and continuous states are also performed to check the Thomas–Kuhn–Reiche rule. In the calculation, only 256 grid points are used, the diagonalization for each angular momentum takes just a few minutes of CPU time on a desktop PC. This economic computing requirement would make it much easier to extend to more complicated problems. We then use the stagger leap-frog algorithm for the time-evolution [14]. This algorithm is explicit and accurate to second-order in time step, hence, the propagation is faster and more efficient than other sophisticated methods such as Runge–Kutta or Crank–Nicholson algorithms.

The rest of the paper is organized as follows: In Section 2, we derive the formulation of the momentum space equation for wave functions. Also, the correction of finite coordinate range on Coulomb kernel and the stagger leap-frog scheme for time propagation are described. In Section 3, we present the calculated energy levels, wave functions, oscillator strengths, and ATI spectra for several cases. Discussion and conclusions are given in Section 4

2. Formulation

Consider the Schrödinger equation for a spherical symmetric potential $V(r)$ in the coordinate representation:

$$-\frac{1}{2}\nabla^2\Psi(\vec{r}) + V(r)\Psi(\vec{r}) = E\Psi(\vec{r}). \tag{1}$$

By making the Fourier transformation,

$$\Phi(\vec{p}) = 1/(2\pi)^{3/2}\int \Psi(\vec{r})\mathrm{e}^{-\mathrm{i}\vec{p}\cdot\vec{r}}\,\mathrm{d}^3r,$$
$$W(\vec{p}) = 1/(8\pi^3)\int V(\vec{r})\mathrm{e}^{-\mathrm{i}\vec{p}\cdot\vec{r}}\,\mathrm{d}^3r, \tag{2}$$

if the space range is infinite, Eq. (1) can be transformed into the momentum representation:

$$\left[\frac{p^2}{2} - E\right]\Phi(\vec{p}) + \int W(\vec{p}-\vec{q})\Phi(\vec{q})\,\mathrm{d}^3q = 0. \tag{3}$$

The above eigenvalue equation in momentum space is well known in quantum mechanics [15,16]. Specifically for the Coulomb potential $V(\vec{r}) = -Z/r$, we can express the eigenstates as

$$\Phi(\vec{p}) = F_{nl}(p)Y_{lm}(\Omega_p), \tag{4}$$

the radial equation of the momentum wave function then becomes

$$\left[\frac{p^2}{2} - E\right]F_{nl}(p) + \int q^2K_l(p,q)F_{nl}(q)\,\mathrm{d}q = 0. \tag{5}$$

The kernel K_l in the above equation can be expressed in terms of Legendre functions of the second kind Q_l:

$$K_l(p,q) = -\frac{Z}{\pi pq}Q_l\left(\frac{p^2+q^2}{2pq}\right), \tag{6}$$

and

$$Q_l(z) = \frac{1}{2}\int_{-1}^{1}\frac{1}{z-x}P_l(x)\,\mathrm{d}x, \tag{7}$$

where P_l is the Legendre function of the first kind. The analytic solution for bound states was given by Fock [6]. Direct numerical solution for the equation is not straightforward due to the singularity in $Q_l(z)$ when $z = \frac{p^2+q^2}{2pq} = 1$, or equivalently, when $p = q$. Lande proposed a clever regularization method to manipulate the kernel term as follows [7]:

$$\begin{aligned}&\int q^2K_l(p,q)F_{nl}(q)\,\mathrm{d}q\\ &\quad= \int K_l(p,q)\left[q^2F_{nl}(q) - p^2F_{nl}(p)/P_l(z)\right]\mathrm{d}q\\ &\qquad+ p^2F_{nl}(p)\int\frac{K_l(p,q)}{P_l(z)}\,\mathrm{d}q.\end{aligned} \tag{8}$$

The first term on the right-hand side is now vanishing at $z = 1$ (that is, $p = q$), and the last term is finite and can be calculated iteratively from $l = 0$ [7,8]. With such technique, a basis expansion method with thousands of terms was successfully used to solve for the bound states in momentum space [9]. It was shown that by using the Gauss–Legendre grids and transform the integral equation into matrix equation, the singularity can be avoided. A grid of thousands points were used to find some bound energy levels of hydrogenic systems accurately [10]. For more general purposes, such as the problem of intense lasers on atoms, such basis functions would be inefficient, especially when continuous states are also needed. We will show how to use far less grid points to construct a good representation for the hydrogenic wave functions, not just for bound states but also for continuum states in the momentum space.

In real calculations, we deal only with finite volume instead of the infinite range in the analytical formulation. The validity of the momentum space Schrödinger equation (3) is subject to a certain condition, namely,

$$1/(8\pi^3)\int_{-L_x}^{L_x}\mathrm{d}x\int_{-L_y}^{L_y}\mathrm{d}y\int_{-L_z}^{L_z}\mathrm{d}z\,\mathrm{e}^{i\vec{p}\cdot\vec{r}} = \frac{\sin(p_xL_x)}{\pi p_x}\frac{\sin(p_yL_y)}{\pi p_y}\frac{\sin(p_zL_z)}{\pi p_z} \cong \delta(p_x)\delta(p_y)\delta(p_z). \tag{9}$$

We know that the condition holds only if the box size $L_xL_yL_z$ is large enough. This point is important as it will modify $W(\vec{p})$ in Eq. (2) for finite box. Considering the hydrogenic potential in spherical coordinates with the maximum radius R in the numerical calculation, the appropriate momentum space form of the Coulomb kernel will then be:

$$W(\vec{p}) = \begin{cases} \frac{\cos(pR)-1}{2\pi^2p^2} & \text{if } p \neq 0, \\ \frac{-R^2}{4\pi^2} & \text{otherwise,} \end{cases} \tag{10}$$

where p is the magnitude of $\vec{p}$. In contrast, the form of the kernel with an infinite box size is given as

$$W(\vec{p}) = \frac{-1}{2\pi^2p^2}. \tag{11}$$

Expanding the modified kernel in Legendre function:

$$W(\vec{p}-\vec{q}) = \sum_{l=0} a_l(p,q)P_l(\cos\gamma), \tag{12}$$

where γ is the angle between $\vec{p}$ and $\vec{q}$, we have

$$a_l(p,q) = \frac{2l+1}{2}\int_{-1}^{1} W(\vec{p}-\vec{q})P_l(x)\,\mathrm{d}x. \tag{13}$$

The above integration can be carried out efficiently by using the Gaussian quadrature [17] with a controlled accuracy. Note that, the singularity in $W(\vec{p}-\vec{q})$ will now happen only at $p=q$ and $\gamma=0$, instead of at $p=q$ in Q_l. Thus, the singularity is less severe and easier to handle. Actually, it does not cause any trouble by using the Gaussian quadrature.

Expanding $P_l(\cos\gamma)$ in spherical harmonics and integrating out the angular part of $\Phi(\vec{p})$, we obtain the radial equation:

$$\left[\frac{p^2}{2}-E\right]F_{nl}(p) + \frac{4\pi}{2l+1}\int_0^{p_{\max}} a_l(p,q)F_{nl}(q)q^2\,\mathrm{d}q = 0. \tag{14}$$

By choosing appropriate grids of p, the above equation becomes a matrix eigenvalue problem. Also, since $p^2/2$ corresponds to the kinetic energy of electron, a finite value is sufficient. Hence, the grids p will be finite-ranged naturally. We may choose its maximum value $p_{\max}$ according to the range of the electron kinetic energy we need. For the radial coordinate p, we further map the range $x\in[-1,1]$ into $[0,p_{\max}]$ by using

$$p = p(x) = L\frac{1+x}{1-x+\alpha}, \tag{15}$$

where $\alpha = 2L/p_{\max}$ and L is the mapping parameter. The collocation points $\{x_k\}$ and the corresponding weights $\{w_k\}$ are determined through the Gauss–Legendre–Lobatto quadrature. The method is especially useful for Coulomb problems [11]. We can switch to denser grids in region of smaller momentum by choosing smaller L or vice versa. This will be an advantage for bound states (more extended in p) or continuous states (photoelectron spectra). With this choice of momentum grids, the discrete eigenvalue equation becomes:

$$\left[\frac{p_i^2}{2}-E\right]F_{nl}(p_i) + \frac{4\pi}{2l+1}\sum_{j=1}^{N} w_j a_l(p_i,q_j)q_j^2F_{nl}(q_j)q'(x_j) = 0, \quad i=1,2,3,\ldots,N; \tag{16}$$

where q_j, $q'(x_j)$ denote $p(x_j)$ and $\mathrm{d}p(x_j)/\mathrm{d}x$ derived from Eq. (15), respectively.

The properties of the numerical eigenset will be presented in the next section. We consider now the time-dependent problem formulation. The Schrödinger equation of the hydrogen atom in a laser pulse under the dipole approximation can be written as

$$i\hbar\frac{\partial\Psi}{\partial t} = \left[H_0 + \vec{A}(t)\cdot\vec{p}\right]\Psi(\vec{p},t), \tag{17}$$

where the electric field $\vec{E}(t) = -\partial\vec{A}(t)/\partial t$. For a linearly polarized field, the magnetic quantum number m is unchanged during the laser pulse and hence is omitted in the formulation below for convenience. We expand Ψ in terms of the obtained pseudocomplete set:

$$\Psi(\vec{p},t) = \sum_{n,l} C_{n,l}(t)F_{nl}(p)Y_{lm}(\hat{p}), \tag{18}$$

where n,l are the principal and orbital quantum numbers, respectively. Integrating out the angular parts, we obtain the followings:

$$i\frac{\mathrm{d}C_{nl}(t)}{\mathrm{d}t} = E_{nl}\cdot C_{nl}(t) + A(t)\sum_{n'}\Big\{b_l\cdot C_{n',l-1}(t) \times\int F_{nl}(p)p^3F_{n',l-1}(p)\,\mathrm{d}p + b_{l+1}\cdot C_{n',l+1}(t)\int F_{nl}(p)p^3F_{n',l+1}(p)\,\mathrm{d}p\Big\}, \tag{19}$$

where

$$b_l \equiv b_{lm} = \sqrt{\frac{(l-m)(l+m)}{(2l-1)(2l+1)}}, \quad \text{for } l=0 \tag{20}$$

and $b_0\equiv 0$.

We decompose $C_{nl}(t)$ into real and imaginary parts. The propagation is then carried out by the stagger leap-frog algorithm with prepared initially state [14].

3. Results

We use $p_{\max}=20$ a.u. and the mapping parameter $L=2$. The value of $p_{\max}^2/2$ corresponds to the largest kinetic energy. This value of $p_{\max}$ is quite large for the kinetic energy, nevertheless, it is necessary for a correct ground state. The ground

Table 1
The magnitudes of errors of the calculated eigenvalues for states (nl) with respect to the exact energy levels $-1/2n^2$

n	E[ns]-exact			E[np]-exact			E[nd]-exact			E[nf]-exact		
	128	256	512	128	256	512	128	256	512	128	256	512
1	8.8[−3]	5.7[−4]	1.6[−4]	–	–	–	–	–	–	–	–	–
2	2.1[−3]	1.0[−4]	2.2[−5]	8.2[−4]	8.2[−6]	6.6[−8]	–	–	–	–	–	–
3	7.2[−4]	3.2[−5]	5.9[−6]	3.7[−4]	3.1[−6]	2.4[−8]	4.2[−5]	5.8[−8]	1.3[−10]	–	–	–
4	3.2[−4]	1.4[−5]	2.5[−6]	1.8[−4]	1.4[−6]	1.1[−8]	2.8[−5]	3.6[−8]	7.8[−11]	1.2[−6]	3.0[−10]	2.2[−13]
5	1.7[−4]	7.3[−6]	1.3[−6]	9.9[−5]	7.5[−7]	5.6[−9]	1.8[−5]	2.1[−8]	4.6[−11]	1.1[−6]	2.6[−10]	1.8[−13]
6	9.7[−5]	4.2[−6]	7.4[−7]	5.9[−5]	4.4[−7]	3.3[−9]	1.1[−5]	1.3[−8]	4.2[−12]	8.0[−7]	1.8[−10]	1.5[−11]
7	6.2[−5]	2.4[−6]	6.6[−7]	3.9[−5]	1.3[−7]	1.6[−7]	7.3[−6]	1.0[−7]	1.2[−7]	4.7[−7]	6.5[−8]	6.5[−8]

The numbers 128, 256 and 512 indicate the number of grid points used in the calculation. $8.8[-3] \equiv 8.8 \times 10^{-3}$.

state is worst case while other states are far more accurately obtained. This is because the ground state is equal to

$$F_{1s} = \frac{2^{5/2}}{\sqrt{\pi}} \frac{1}{(p^2+1)^2}, \tag{21}$$

which is the most diffusive state in momentum space wave functions and needs a larger $p_{\max}$ to attain higher accuracy. We show later in Table 4 that much larger value of $p_{\max}$ is required for the same accuracy by Lande's regularization method. The continuous state wave functions are quite localized and hence need denser grids in smaller values of p. For the accurate continuous states, the value of L should not be large. We found that the results are not sensitive to the choices of L and $p_{\max}$. We use $R = 150.0$ a.u. which satisfies the limiting Dirac δ-function in Eq. (9) very well. The results are also insensitive to the value of R. We do not intend to carry out high precision calculations in this paper. Instead, we propose to develop a tractable and efficient momentum space method, but still reliable enough to simulate quantum dynamics of intense lasers on atoms or molecules while the coordinate space method does not work well.

In the following, we use only 256 grid points for the p-coordinate and calculate the discretized eigenvalue equations. We learn by comparing the results with $L = 1$ and $L = 2$ and found no noticeable difference in eigenstates and time-dependent cases. First, we present in Table 1 the results of some low-lying bound states. The accuracy is quite good. The ground state is accurate up to the fourth decimal place and is the worst case, and the accuracy is up to the 8th significant digit for the $7f$-state. For comparison, we also listed in Table 1 the results with 128 and 512 grid points. All show excellent accuracy for those bound levels. In fact, for the study of quantum dynamics, the use of 128 grid points will be satisfactory if computing time is concerned.

Since we discretized the system, the set of eigenstates is pseudocomplete with a finite number of eigenstates. This makes numerical calculations useful, for though analytic solutions are known, there are an infinite number of states. There are only few bound states obtained for each nl-series numerically. If bound state resonances are important, optimizing the grids and the parameters will provide more bound states with increasing accuracy.

We compared the radial wave functions of $1s$, $3s$, $2p$ and $3d$ with analytic forms listed in Ref. [16]. The accuracy at any grid point is at least 3 significant digits. Based on quantum mechanics, the extent of a momentum wave function is localized in a small range while the corresponding coordinate space wave function extends far away out for higher states. This is an advantage of the momentum space approach, for the highly excited states and continuous states are localized in momentum space.

The next question is how good the generated wave functions are. To address this question, we calculated the oscillator strengths of several states and compared them with the exact results tabulated in Bethe and Salpeter [13]. The oscillator strength for the transition from state (nl) to state $(n'l')$ is given as

$$f_{nl\to n',l+1} = \frac{2(l+1)}{3(2l+1)} \frac{1}{E_{n'} - En} \left| \int p^3 F_{nl}(p) F_{n',l+1}(p) \right|^2, \tag{22}$$

$$f_{nl\to n',l-1} = \frac{2l}{3(2l+1)} \frac{1}{E_{n'} - En} \left| \int p^3 F_{nl}(p) F_{n',l-1}(p) \right|^2. \tag{23}$$

We also tested the well-known Thomas–Reiche–Kuhn sum rule using the generated eigenstates. In Table 2, the oscillator strengths from states $1s$, $2s$, $3s$, $4s$ to states np are listed together with the discrepancies from Bethe and Salpeter's [13]. The summations over simulated finite number of bound states and continuous states agree very well with the exact results. Individual oscillator strength also agrees well. We also perform the calculations of the oscillator strengths from $2p$ and $4f$ states. The results are listed in Tables 3 and 4. With only 256 momentum grid points, we can say that the Hilbert space of the real hydrogen atom has been satisfactorily represented numerically. Higher precision can easily be reached with more grid points and larger value of $p_{\max}$ and R.

For the simulation of intense laser pulses on a hydrogen atom, we assume the electric field pulse is

$$\vec{E}(t) = \hat{z} E_m \sin\omega t \sin^2 \frac{\pi t}{T}, \tag{24}$$

where ω is the laser frequency and T is the pulse duration. T is equal to 2.75 times of the full width at half maximum (FWHM), and the system is initial prepared in the hydrogenic ground state.

In Table 5, we list the four calculated cases of the ATI spectra. Cases I and II were compared to the recent paper of Ref. [4].

Table 2
The oscillator strengths for the transition from ns-state to $n'p$-state

Final	Error($1s$)	B-S	Error($2s$)	B-S	Error($3s$)	B-S	Error($4s$)	B-S
$2p$	−5.92[−4]	0.4162	–	–	−7.31[−5]	−4.1[−2]	−1.92[−4]	−0.009
$3p$	−2.16[−5]	7.91[−2]	−1.46[−3]	0.4349	–	–	−4.79[−4]	−0.097
$4p$	2.01[−6]	2.90[−2]	−1.82[−4]	0.1028	−1.39[−5]	0.484	–	–
$5p$	3.03[−6]	1.39[−2]	−5.17[−5]	4.19[−2]	−2.95[−4]	0.121	3.50[−3]	0.545
$6p$	2.30[−6]	7.80[−3]	−2.12[−5]	2.16[−2]	7.10[−4]	5.2[−2]	−3.13 − 4]	0.138
$7p$	3.38[−6]	4.81[−3]	−6.18[−6]	1.27[−2]	3.30[−4]	2.7[−2]	−4.82[−4]	6.0[−2]
Discrete sum	3.86[−4]	0.5650	5.60[−4]	0.6489	3.71[−3]	0.707	−1.39[−4]	0.752
Continuous sum	1.14[−3]	0.4350	−1.34[−3]	0.3511	−5.99[−3]	0.293	−3.95[−3]	0.248
Total	1.53[−3]	1.000	−7.83[−4]	1.000	−2.56[−3]	1.000	−4.09[−3]	1.000

Error(ns) is the error between the calculated and the corresponding exact results. B-S denotes the results in Ref. [13]. $-5.92[-4] \equiv -5.92 \times 10^{-4}$.

Table 3
The oscillator strength for the transition from the $2p$-state to ns- and nd-states

Final n	Error(ns)	B-S	Error(nd)	B-S
$n = 1$	1.97[−4]	−0.139	–	–
2	–	–	–	–
3	1.01[−4]	1.36[−2]	−9.16[−5]	0.696
4	1.90[−5]	3.04[−3]	5.28[−6]	0.122
5	7.10[−6]	1.21[−3]	4.75[−6]	4.44[−2]
6	3.50[−6]	6.18[−4]	3.00[−6]	2.16[−2]
7	2.15[−6]	3.61[−4]	5.11[−6]	1.23[−2]
Discrete sum	4.80[−4]	−0.119	1.66[−3]	0.928
Continuous sum	−2.15[−4]	0.008	−1.51[−3]	0.183
Total	2.65[−4]	−0.111	1.50[−4]	1.111

Error(nl) is the error between the calculated and the corresponding exact results. B-S denotes the results in Ref. [13]. $1.97[-4] \equiv 1.97 \times 10^{-4}$.

Table 4
The oscillator strength for the transition from $4f$-state to nd- and ng-state

Final n	Error(nd)	B-S	Error(ng)	B-S
$n = 3$	2.03[−4]	−0.727	–	–
4	–	–	–	–
5	−1.28[−4]	0.009	8.00[−4]	1.345
6	−1.70[−5]	1.6[−3]	−6.46[−5]	0.183
7	6.46[−5]	0.0005	3.83[−4]	0.058
Discrete sum	9.40[−5]	−0.715	6.64[−3]	1.658
Continuous sum	−3.77[−4]	0.001	−6.35[−3]	0.056
Total	−2.83[−4]	−0.714	2.90[−4]	1.714

Error(nl) is the error between the calculated and the exact results. B-S denotes the results in Ref. [13]. $2.03[-4] \equiv 2.03 \times 10^{-4}$.

In these two cases, the laser intensity is not very high so that the ionization probability is small. The pulse duration is set to 20 optical cycles and FWHM is about 10 fs. We perform simulation in case III with a stronger field that the atom is almost totally ionized. The corresponding calculation in coordinate space will be quite hard. Case IV simulates an experimental data [18]. The pulse duration is in sub-picosecond range. The computation was regarded not feasible before [12]. In Fig. 1, we present the ATI spectrum for the case of peak intensity 10^{14} watt/cm^2 with T equal to 20 optical cycles (26.64 fs). At the end of pulse, the probability of excitation into angular momentum states $l = 8$ is 1.89×10^{-7}, and to states of $l = 11$ is 1.5×10^{-11}. Thus, $l = 0, 1, \ldots, 11$ that we used in the expansion are more than enough and guarantee the convergence of calculations. The total number of eigenstates in the basis state is 3072 while 73 of them are bound states. The ionization probability is 2.15% only. We plot in both linear and log scales for the probability density $P(E)$ with respect to photoelectron energy in eV. $P(E)$ is defined through

$$\int P(E)\,\mathrm{d}E = 1. \tag{25}$$

Also we define the threshold energy as

Table 5
The four ATI spectra cases

Case	λ (nm)	I_{peak} (w/cm^2)	T (fs)	$l_{\max}$	$P_{l\,\max}$	P_{ionized}
I	400	10^{14}	26.6	11	1.5×10^{-11}	2.15%
II	400	2×10^{14}	26.6	14	3.7×10^{-11}	7.23%
III	400	10^{15}	26.6	39	2.5×10^{-10}	91.97%
IV	608	10^{14}	405	29	4.6×10^{-10}	2.63%

λ is the laser wavelength. I_{peak} is the peak intensity of the laser field. T is the pulse duration in femtoseconds. The angular momenta used in each case are $l = 0, 1, \ldots, l_{\max}$. $P_{l\,\max}$ is the probability of the final state in angular momentum stats of $l = l_{\max}$. P_{ionized} is the ionization probability.

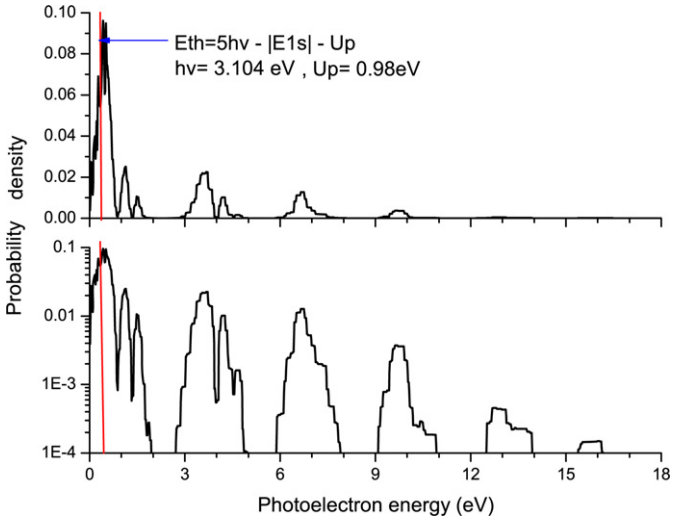

Fig. 1. ATI spectrum for case I. The red vertical line depicts the threshold energy. The first three dominant ATI peaks are to be compared with Ref. [4]. More peaks are shown in logarithmic scale. (For colours see the web version of this article.)

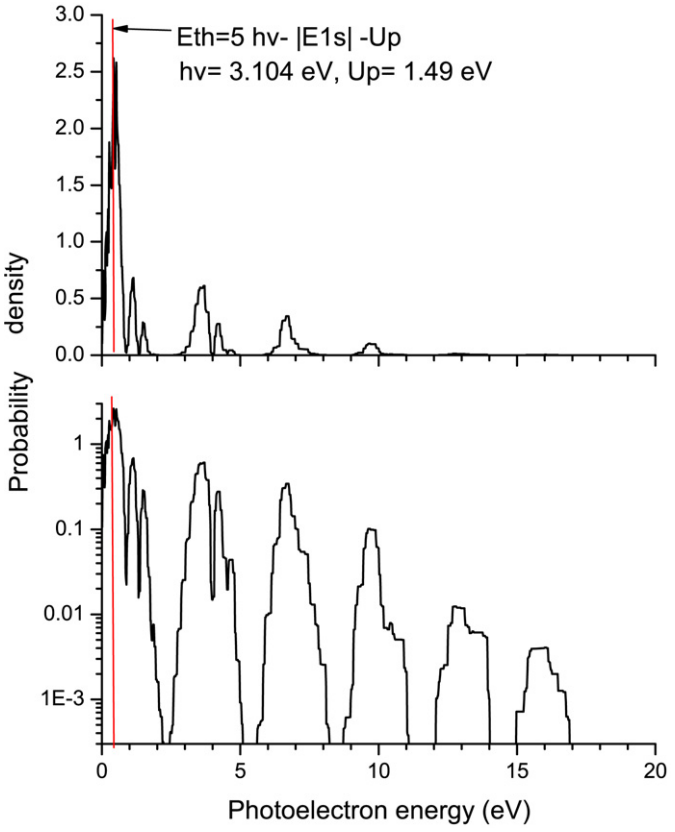

Fig. 2. ATI spectrum for case II. The results are to be compared with Ref. [4].

$$E_{th} = N_{\min}\hbar\omega - |E_{1s}| - U_p, \tag{26}$$

where E_{1s} is the energy of the ground state, $U_p = E_m^2/4\omega^2$, the ponderomotive energy. $N_{\min}$ is the minimum number of photons absorbed by the atom such that the threshold energy becomes positive. There is no ATI peak for a negative threshold energy [5]. Fig. 2 depicts the results with 2×10^{14} watt/cm^2 peak laser intensity. The logarithmic plot shows more minor peaks that are invisible in linear scale. Note that the substructures in main ATI peaks are due to the Freeman resonances in the short pulse case [19].

In Fig. 3 we show the strong field result that is hard to calculate in coordinate space. The ponderomotive energy is now 74.45 eV and needs at least 29 photons to make the threshold energy positive. The first ATI peak is suppressed and more ATI peaks show up. These are the typical effects of *peak suppression* and *peak switching* in strong field physics [3]. Since the pulse duration is short, the resonance structures also appeared. Finally in Fig. 4 we show the ATI spectrum of the hydrogen atom under a pulse of 200 optical cycles (405 fs) to compare with the experimental results [18]. Since the experimental parameters usually cannot be unlimited precise, the direct comparison between experimental and theoretical results are not straightforward. We use the estimated intensity and pulse duration. The pulse duration is quite long and the calculation is able to show the dominant features of the experimental ATI spectrum.

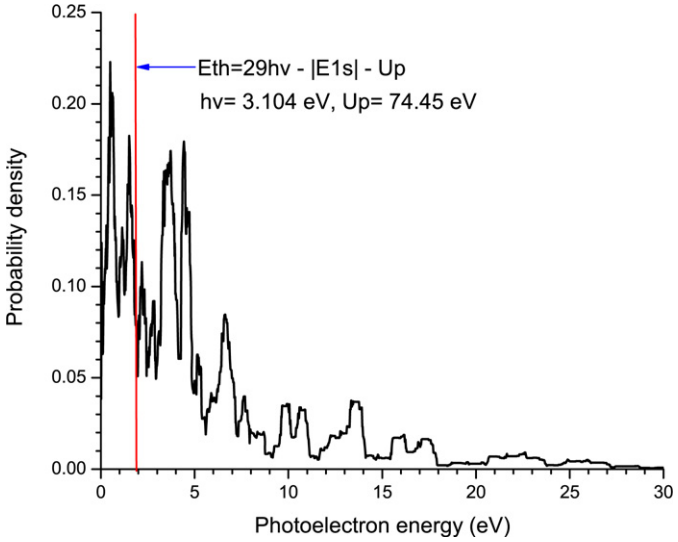

Fig. 3. ATI spectrum for case III. The laser intensity is Peta watt/cm^2, which is quite strong. Peak suppression and switching characteristics appear. Since the pulse duration is short, Freeman resonances are associated with the main ATI peaks.

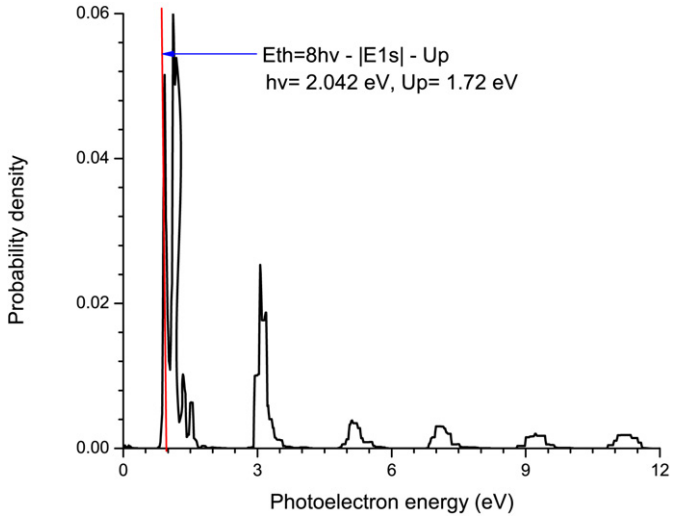

Fig. 4. Simulations to compare with experiment Ref. [18]. Main characteristics of experimental results are obtained.

4. Discussion and conclusions

We have developed an efficient and accurate method of the calculation for wave functions of hydrogen atom in momentum space. To our knowledge, there are several other studies on this problem without correcting the potential kernel due to the finite coordinate size [5,7,9,10]. This modification of the Coulomb kernel is essential. In Table 6 we tabulated the energy levels of ns-states, *with* (labeled as $R = 150$) or *without* (labeled as *without* R) the correction of R to the potential kernel, or using the Lande subtraction with the same number of grid points and optimized parameters. We can see the drastic improvement to the energy levels when the kernel is corrected. And also, with the same grids and $p_{\max}$, the Lande's subtraction method does not give good results; only with

Table 6
Comparison of the calculated energy levels of the ns-state by several methods

State	$R = 150$	*without R*	Lande I	Lande II
1s	0.5006	0.5896	0.5338	0.5013
2s	0.1255	0.1726	0.1335	0.1253
3s	5.559[−2]	9.250[−2]	5.934[−2]	5.570[−2]
4s	3.126[−2]	6.311[−2]	3.339[−2]	3.133[−2]
5s	2.001[−2]	4.883[−2]	2.138[−2]	2.006[−2]
6s	1.389[−2]	4.065[−2]	1.485[−2]	1.393[−2]

$R = 150$ a.u. are results with grids described in Table 1, results from the traditional potential kernel with the same grids are denoted as "*without R*". The results with Lande subtraction at the same grids, that is, 256 grid points and $p_{\max} = 20$ a.u., are denoted as Lande I. Lande II are results with Lande method at $p_{\max} = 500$ a.u. and 512 grid points. $5.559[-2] \equiv 5.559 \times 10^{-2}$. The negative sign to every energy level is omitted. The exact eigenvalues are $-E_n = 0.5/n^2$.

512 grid points and $p_{\max} = 500$ a.u. can we generate moderately accurate eigenvalues. It takes thousands of grid points to generate accurate low-lying bound states with Lande's regularization. This agrees with Refs. [9,10]. However, such large value of $p_{\max}$ is not meaningful for too large in kinetic energy and the necessity of a large number of grid points is another disadvantage for future applications to intense field problems. Thus, the finite-R correction to the potential kernel is critical to the momentum space formulation. The use of the Gauss–Legendre quadrature enables us to bypass the Lande subtraction and greatly simplifies the calculation. With a moderate number of grid points, the Hilbert space of the hydrogen hamiltonian is well represented.

With the economic-sized basis set of momentum space wave functions and the efficient stagger leap-frog time evolution algorithm, we are able to calculate the ATI photoelectron spectra. We elucidate the capability of this method with the atom either under a very high intensity or a very long duration laser pulse to show the nice features. There is no loss of the continuous part of the wave functions, unlike filtering function employed in coordinate space method to prevent boundary reflection. Further applications of the method to intense laser pulses on atoms and molecules will be presented in the future.

Acknowledgements

The author thanks helpful discussions with Professor Chii-Dong Lin. Technical assistance of Yun-Min Lee, and improvement of the writing by Bor-Yuan are gratefully acknowledged. The work is supported by the National Science Councilof Taiwan under contract number NSC95-2112-M009-028-MY2, the MOE/ATU Program, and the Elite Foundation.

References

[1] P. Agostini, F. Fabre, G. Mainfray, G. Petite, N.K. Rahman, Phys. Rev. Lett. 42 (1979) 1127.
[2] For a review on experimental investigations, see for example, R.P. Freeman, P.H. Bucksbaum, J. Phys. B: At. Mol. Opt. Phys. 24 (1991) 325;
on theoretical aspects, see K. Kulander, A. L'Huillier (Eds.), Theory of high-order processes in atoms in intense laser fields, J. Opt. Soc. Am. B 7 (1990) 407;
D.B. Milošević, G.G. Paulus, D. Bauer, W. Becker, J. Phys. B: At. Mol. Opt. Phys. 39 (2006) R203.
[3] S.-I Chu, J. Cooper, Phys. Rev. A 32 (1985) 2769;
M. Dörr, R.M. Potvliege, R. Shakeshaft, Phys. Rev. A 41 (1990) 558;
X. Tang, S. Basile, Phys. Rev. A 44 (1991) R1454;
M. Pont, D. Proulx, R. Shakeshaft, Phys. Rev. A 44 (1991) 4486.
[4] Z. Chen, T. Morishita, A.T. Le, M. Wicherhauser, X.M. Tong, C.D. Lin, Phys. Rev. A 74 (2006) 053405.
[5] U.-L. Pen, T.F. Jiang, Phys. Rev. A 46 (1992) 4297;
U.-L. Pen, T.F. Jiang, Phys. Rev. A 53 (1996) 623.
[6] V.A. Fock, Z. Physik 98 (1935) 145.
[7] Y.R. Kwon, F. Tabakin, Phys. Rev. C 18 (1978) 932 (Ref. 8).
[8] I.A. Ivanov, J. Mitroy, Comput. Phys. Comm. 134 (2001) 317.
[9] J.W. Norbury, K.M. Maung, D.E. Kahana, Phys. Rev. A 50 (1994) 2075.
[10] A. Tang, J.W. Norbury, Phys. Rev. E 63 (2001) 066703.
[11] J. Wang, S.I. Chu, C. Laughlin, Phys. Rev. A 50 (1994) 3208.
[12] K. Burnett, V.C. Reed, P.L. Knight, J. Phys. B 26 (1993) 561;
H. Rottke, B. Wolff-Rottke, D. Feldmann, K.H. Welge, M. Dörr, R.M. Potvliege, R. Shakeshaft, Phys. Rev. A 49 (1994) 4837.
[13] H.A. Bethe, E.E. Salpeter, Quantum mechanics of One- and Two-electron Atoms, Plenum Publishing, New York, 1977 (Sec. 63, Table 14).
[14] P.B. Visscher, Comp. in Phys. (Nov/Dec. 1991) 596.
[15] S. Flügge, Practical Quantum Mechanics, Springer-Verlag, New York, 1974 (Problem 77, 78).
[16] B.H. Bransden, C.J. Joachain, Physics of Atoms and Molecules, second ed., Prentice-Hall, New York, 2003 (Appendix 5).
[17] W.H. Press, S.A. Teukolsky, W.T. Vetterling, B.P. Flannery, Numerical Recipes in FORTRAN, second ed., Cambridge Univ. Press, New York, 1992.
[18] H. Rottke, B. Wolff, M. Brickwedde, D. Feldmann, K.H. Welge, Phys. Rev. Lett. 64 (1990) 404.
[19] R.R. Freeman, P.H. Bucksbaum, H. Milchberg, S. Darack, D. Schumacher, M.E. Geusic, Phys. Rev. Lett. 59 (1987) 1092.